

Measurements of the rare decays $B \rightarrow K\ell^+\ell^-$ and $B \rightarrow K^*\ell^+\ell^-$

The *BABAR* Collaboration

July 1, 2005

Abstract

We present measurements of the flavor-changing neutral current decays $B \rightarrow K\ell^+\ell^-$ and $B \rightarrow K^*\ell^+\ell^-$, where $\ell^+\ell^-$ is either an e^+e^- or $\mu^+\mu^-$ pair. The data sample comprises 229×10^6 $\Upsilon(4S) \rightarrow B\bar{B}$ decays collected with the *BABAR* detector at the PEP-II e^+e^- storage ring. We measure the branching fractions

$$\mathcal{B}(B \rightarrow K\ell^+\ell^-) = (0.34 \pm 0.07 \pm 0.03) \times 10^{-6}$$

$$\mathcal{B}(B \rightarrow K^*\ell^+\ell^-) = (0.78_{-0.17}^{+0.19} \pm 0.12) \times 10^{-6},$$

the direct CP asymmetries of these decays, and the relative abundances of decays to electrons and muons.

Contributed to the XXIIst International Symposium on Lepton and Photon Interactions at High Energies, 6/27 — 7/5/2005, Uppsala, Sweden

Stanford Linear Accelerator Center, Stanford University, Stanford, CA 94309

Work supported in part by Department of Energy contract DE-AC03-76SF00515.

The BABAR Collaboration,

B. Aubert, R. Barate, D. Boutigny, F. Couderc, Y. Karyotakis, J. P. Lees, V. Poireau, V. Tisserand,
A. Zghiche

Laboratoire de Physique des Particules, F-74941 Annecy-le-Vieux, France

E. Grauges

IFAE, Universitat Autònoma de Barcelona, E-08193 Bellaterra, Barcelona, Spain

A. Palano, M. Pappagallo, A. Pompili

Università di Bari, Dipartimento di Fisica and INFN, I-70126 Bari, Italy

J. C. Chen, N. D. Qi, G. Rong, P. Wang, Y. S. Zhu

Institute of High Energy Physics, Beijing 100039, China

G. Eigen, I. Ofte, B. Stugu

University of Bergen, Institute of Physics, N-5007 Bergen, Norway

G. S. Abrams, M. Battaglia, A. B. Breon, D. N. Brown, J. Button-Shafer, R. N. Cahn, E. Charles,
C. T. Day, M. S. Gill, A. V. Gritsan, Y. Groysman, R. G. Jacobsen, R. W. Kadel, J. Kadyk, L. T. Kerth,
Yu. G. Kolomensky, G. Kukartsev, G. Lynch, L. M. Mir, P. J. Oddone, T. J. Orimoto, M. Pripstein,
N. A. Roe, M. T. Ronan, W. A. Wenzel

Lawrence Berkeley National Laboratory and University of California, Berkeley, California 94720, USA

M. Barrett, K. E. Ford, T. J. Harrison, A. J. Hart, C. M. Hawkes, S. E. Morgan, A. T. Watson

University of Birmingham, Birmingham, B15 2TT, United Kingdom

M. Fritsch, K. Goetzen, T. Held, H. Koch, B. Lewandowski, M. Pelizaeus, K. Peters, T. Schroeder,
M. Steinke

Ruhr Universität Bochum, Institut für Experimentalphysik 1, D-44780 Bochum, Germany

J. T. Boyd, J. P. Burke, N. Chevalier, W. N. Cottingham

University of Bristol, Bristol BS8 1TL, United Kingdom

T. Cuhadar-Donszelmann, B. G. Fulsom, C. Hearty, N. S. Knecht, T. S. Mattison, J. A. McKenna

University of British Columbia, Vancouver, British Columbia, Canada V6T 1Z1

A. Khan, P. Kyberd, M. Saleem, L. Teodorescu

Brunel University, Uxbridge, Middlesex UB8 3PH, United Kingdom

A. E. Blinov, V. E. Blinov, A. D. Bukin, V. P. Druzhinin, V. B. Golubev, E. A. Kravchenko,
A. P. Onuchin, S. I. Serebnyakov, Yu. I. Skovpen, E. P. Solodov, A. N. Yushkov

Budker Institute of Nuclear Physics, Novosibirsk 630090, Russia

D. Best, M. Bondioli, M. Bruinsma, M. Chao, S. Curry, I. Eschrich, D. Kirkby, A. J. Lankford, P. Lund,
M. Mandelkern, R. K. Mommsen, W. Roethel, D. P. Stoker

University of California at Irvine, Irvine, California 92697, USA

C. Buchanan, B. L. Hartfiel, A. J. R. Weinstein

University of California at Los Angeles, Los Angeles, California 90024, USA

S. D. Foulkes, J. W. Gary, O. Long, B. C. Shen, K. Wang, L. Zhang
University of California at Riverside, Riverside, California 92521, USA

D. del Re, H. K. Hadavand, E. J. Hill, D. B. MacFarlane, H. P. Paar, S. Rahatlou, V. Sharma
University of California at San Diego, La Jolla, California 92093, USA

J. W. Berryhill, C. Campagnari, A. Cunha, B. Dahmes, T. M. Hong, M. A. Mazur, J. D. Richman,
W. Verkerke
University of California at Santa Barbara, Santa Barbara, California 93106, USA

T. W. Beck, A. M. Eisner, C. J. Flacco, C. A. Heusch, J. Kroseberg, W. S. Lockman, G. Nesom, T. Schalk,
B. A. Schumm, A. Seiden, P. Spradlin, D. C. Williams, M. G. Wilson
University of California at Santa Cruz, Institute for Particle Physics, Santa Cruz, California 95064, USA

J. Albert, E. Chen, G. P. Dubois-Felsmann, A. Dvoretzki, D. G. Hitlin, I. Narsky, T. Piatenko,
F. C. Porter, A. Ryd, A. Samuel
California Institute of Technology, Pasadena, California 91125, USA

R. Andreassen, S. Jayatilleke, G. Mancinelli, B. T. Meadows, M. D. Sokoloff
University of Cincinnati, Cincinnati, Ohio 45221, USA

F. Blanc, P. Bloom, S. Chen, W. T. Ford, J. F. Hirschauer, A. Kreisel, U. Nauenberg, A. Olivas,
P. Rankin, W. O. Ruddick, J. G. Smith, K. A. Ulmer, S. R. Wagner, J. Zhang
University of Colorado, Boulder, Colorado 80309, USA

A. Chen, E. A. Eckhart, J. L. Harton, A. Soffer, W. H. Toki, R. J. Wilson, Q. Zeng
Colorado State University, Fort Collins, Colorado 80523, USA

D. Altenburg, E. Feltresi, A. Hauke, B. Spaan
Universität Dortmund, Institut für Physik, D-44221 Dortmund, Germany

T. Brandt, J. Brose, M. Dickopp, V. Klose, H. M. Lacker, R. Nogowski, S. Otto, A. Petzold, G. Schott,
J. Schubert, K. R. Schubert, R. Schwierz, J. E. Sundermann
Technische Universität Dresden, Institut für Kern- und Teilchenphysik, D-01062 Dresden, Germany

D. Bernard, G. R. Bonneaud, P. Grenier, S. Schrenk, Ch. Thiebaut, G. Vasileiadis, M. Verderi
Ecole Polytechnique, LLR, F-91128 Palaiseau, France

D. J. Bard, P. J. Clark, W. Gradl, F. Muheim, S. Playfer, Y. Xie
University of Edinburgh, Edinburgh EH9 3JZ, United Kingdom

M. Andreotti, V. Azzolini, D. Bettoni, C. Bozzi, R. Calabrese, G. Cibinetto, E. Luppi, M. Negrini,
L. Piemontese
Università di Ferrara, Dipartimento di Fisica and INFN, I-44100 Ferrara, Italy

F. Anulli, R. Baldini-Ferrolì, A. Calcaterra, R. de Sangro, G. Finocchiaro, P. Patteri, I. M. Peruzzi,¹
M. Piccolo, A. Zallo
Laboratori Nazionali di Frascati dell'INFN, I-00044 Frascati, Italy

¹Also with Università di Perugia, Dipartimento di Fisica, Perugia, Italy

A. Buzzo, R. Capra, R. Contri, M. Lo Vetere, M. Macri, M. R. Monge, S. Passaggio, C. Patrignani,
E. Robutti, A. Santroni, S. Tosi

Università di Genova, Dipartimento di Fisica and INFN, I-16146 Genova, Italy

G. Brandenburg, K. S. Chaisanguanthum, M. Morii, E. Won, J. Wu

Harvard University, Cambridge, Massachusetts 02138, USA

R. S. Dubitzky, U. Langenegger, J. Marks, S. Schenk, U. Uwer

Universität Heidelberg, Physikalisches Institut, Philosophenweg 12, D-69120 Heidelberg, Germany

W. Bhimji, D. A. Bowerman, P. D. Dauncey, U. Egede, R. L. Flack, J. R. Gaillard, G. W. Morton,
J. A. Nash, M. B. Nikolich, G. P. Taylor, W. P. Vazquez

Imperial College London, London, SW7 2AZ, United Kingdom

M. J. Charles, W. F. Mader, U. Mallik, A. K. Mohapatra

University of Iowa, Iowa City, Iowa 52242, USA

J. Cochran, H. B. Crawley, V. Eyges, W. T. Meyer, S. Prell, E. I. Rosenberg, A. E. Rubin, J. Yi

Iowa State University, Ames, Iowa 50011-3160, USA

N. Arnaud, M. Davier, X. Giroux, G. Grosdidier, A. Höcker, F. Le Diberder, V. Lepeltier, A. M. Lutz,
A. Oyanguren, T. C. Petersen, M. Pierini, S. Plaszczynski, S. Rodier, P. Roudeau, M. H. Schune,
A. Stocchi, G. Wormser

Laboratoire de l'Accélérateur Linéaire, F-91898 Orsay, France

C. H. Cheng, D. J. Lange, M. C. Simani, D. M. Wright

Lawrence Livermore National Laboratory, Livermore, California 94550, USA

A. J. Bevan, C. A. Chavez, I. J. Forster, J. R. Fry, E. Gabathuler, R. Gamet, K. A. George,
D. E. Hutchcroft, R. J. Parry, D. J. Payne, K. C. Schofield, C. Touramanis

University of Liverpool, Liverpool L69 7ZE, United Kingdom

C. M. Cormack, F. Di Lodovico, W. Menges, R. Sacco

Queen Mary, University of London, E1 4NS, United Kingdom

C. L. Brown, G. Cowan, H. U. Flaecher, M. G. Green, D. A. Hopkins, P. S. Jackson, T. R. McMahon,
S. Ricciardi, F. Salvatore

University of London, Royal Holloway and Bedford New College, Egham, Surrey TW20 0EX, United Kingdom

D. Brown, C. L. Davis

University of Louisville, Louisville, Kentucky 40292, USA

J. Allison, N. R. Barlow, R. J. Barlow, C. L. Edgar, M. C. Hodgkinson, M. P. Kelly, G. D. Lafferty,
M. T. Naisbit, J. C. Williams

University of Manchester, Manchester M13 9PL, United Kingdom

C. Chen, W. D. Hulsbergen, A. Jawahery, D. Kovalskyi, C. K. Lae, D. A. Roberts, G. Simi

University of Maryland, College Park, Maryland 20742, USA

G. Blaylock, C. Dallapiccola, S. S. Hertzbach, R. Kofler, V. B. Koptchev, X. Li, T. B. Moore, S. Saremi,
H. Staengle, S. Willocq

University of Massachusetts, Amherst, Massachusetts 01003, USA

R. Cowan, K. Koeneke, G. Sciolla, S. J. Sekula, M. Spitznagel, F. Taylor, R. K. Yamamoto
*Massachusetts Institute of Technology, Laboratory for Nuclear Science, Cambridge, Massachusetts 02139,
USA*

H. Kim, P. M. Patel, S. H. Robertson
McGill University, Montréal, Quebec, Canada H3A 2T8

A. Lazzaro, V. Lombardo, F. Palombo
Università di Milano, Dipartimento di Fisica and INFN, I-20133 Milano, Italy

J. M. Bauer, L. Cremaldi, V. Eschenburg, R. Godang, R. Kroeger, J. Reidy, D. A. Sanders, D. J. Summers,
H. W. Zhao

University of Mississippi, University, Mississippi 38677, USA

S. Brunet, D. Côté, P. Taras, B. Viaud
Université de Montréal, Laboratoire René J. A. Lévesque, Montréal, Quebec, Canada H3C 3J7

H. Nicholson
Mount Holyoke College, South Hadley, Massachusetts 01075, USA

N. Cavallo,² G. De Nardo, F. Fabozzi,² C. Gatto, L. Lista, D. Monorchio, P. Paolucci, D. Piccolo,
C. Sciacca

Università di Napoli Federico II, Dipartimento di Scienze Fisiche and INFN, I-80126, Napoli, Italy

M. Baak, H. Bulten, G. Raven, H. L. Snoek, L. Wilden
*NIKHEF, National Institute for Nuclear Physics and High Energy Physics, NL-1009 DB Amsterdam, The
Netherlands*

C. P. Jessop, J. M. LoSecco
University of Notre Dame, Notre Dame, Indiana 46556, USA

T. Allmendinger, G. Benelli, K. K. Gan, K. Honscheid, D. Hufnagel, P. D. Jackson, H. Kagan, R. Kass,
T. Pulliam, A. M. Rahimi, R. Ter-Antonyan, Q. K. Wong

Ohio State University, Columbus, Ohio 43210, USA

J. Brau, R. Frey, O. Igonkina, M. Lu, C. T. Potter, N. B. Sinev, D. Strom, J. Strube, E. Torrence
University of Oregon, Eugene, Oregon 97403, USA

F. Galeazzi, M. Margoni, M. Morandin, M. Posocco, M. Rotondo, F. Simonetto, R. Stroili, C. Voci
Università di Padova, Dipartimento di Fisica and INFN, I-35131 Padova, Italy

M. Benayoun, H. Briand, J. Chauveau, P. David, L. Del Buono, Ch. de la Vaissière, O. Hamon,
M. J. J. John, Ph. Leruste, J. Malclès, J. Ocariz, L. Roos, G. Therin
*Universités Paris VI et VII, Laboratoire de Physique Nucléaire et de Hautes Energies, F-75252 Paris,
France*

²Also with Università della Basilicata, Potenza, Italy

P. K. Behera, L. Gladney, Q. H. Guo, J. Panetta
University of Pennsylvania, Philadelphia, Pennsylvania 19104, USA

M. Biasini, R. Covarelli, S. Pacetti, M. Pioppi
Università di Perugia, Dipartimento di Fisica and INFN, I-06100 Perugia, Italy

C. Angelini, G. Batignani, S. Bettarini, F. Bucci, G. Calderini, M. Carpinelli, R. Cenci, F. Forti,
M. A. Giorgi, A. Lusiani, G. Marchiori, M. Morganti, N. Neri, E. Paoloni, M. Rama, G. Rizzo, J. Walsh
Università di Pisa, Dipartimento di Fisica, Scuola Normale Superiore and INFN, I-56127 Pisa, Italy

M. Haire, D. Judd, D. E. Wagoner
Prairie View A&M University, Prairie View, Texas 77446, USA

J. Biesiada, N. Danielson, P. Elmer, Y. P. Lau, C. Lu, J. Olsen, A. J. S. Smith, A. V. Telnov
Princeton University, Princeton, New Jersey 08544, USA

F. Bellini, G. Cavoto, A. D'Orazio, E. Di Marco, R. Faccini, F. Ferrarotto, F. Ferroni, M. Gaspero, L. Li
Gioi, M. A. Mazzoni, S. Morganti, G. Piredda, F. Polci, F. Safai Tehrani, C. Voena
Università di Roma La Sapienza, Dipartimento di Fisica and INFN, I-00185 Roma, Italy

H. Schröder, G. Wagner, R. Waldi
Universität Rostock, D-18051 Rostock, Germany

T. Adye, N. De Groot, B. Franek, G. P. Gopal, E. O. Olaiya, F. F. Wilson
Rutherford Appleton Laboratory, Chilton, Didcot, Oxon, OX11 0QX, United Kingdom

R. Aleksan, S. Emery, A. Gaidot, S. F. Ganzhur, P.-F. Giraud, G. Graziani, G. Hamel de Monchenault,
W. Kozanecki, M. Legendre, G. W. London, B. Mayer, G. Vasseur, Ch. Yèche, M. Zito
DSM/Daphnia, CEA/Saclay, F-91191 Gif-sur-Yvette, France

M. V. Purohit, A. W. Weidemann, J. R. Wilson, F. X. Yumiceva
University of South Carolina, Columbia, South Carolina 29208, USA

T. Abe, M. T. Allen, D. Aston, N. van Bakel, R. Bartoldus, N. Berger, A. M. Boyarski, O. L. Buchmueller,
R. Claus, J. P. Coleman, M. R. Convery, M. Cristinziani, J. C. Dingfelder, D. Dong, J. Dorfan, D. Dujmic,
W. Dunwoodie, S. Fan, R. C. Field, T. Glanzman, S. J. Gowdy, T. Hadig, V. Halyo, C. Hast, T. Hryn'ova,
W. R. Innes, M. H. Kelsey, P. Kim, M. L. Kocian, D. W. G. S. Leith, J. Libby, S. Luitz, V. Luth,
H. L. Lynch, H. Marsiske, R. Messner, D. R. Muller, C. P. O'Grady, V. E. Ozcan, A. Perazzo, M. Perl,
B. N. Ratcliff, A. Roodman, A. A. Salnikov, R. H. Schindler, J. Schwiening, A. Snyder, J. Stelzer, D. Su,
M. K. Sullivan, K. Suzuki, S. Swain, J. M. Thompson, J. Va'vra, M. Weaver, W. J. Wisniewski,
M. Wittgen, D. H. Wright, A. K. Yarritu, K. Yi, C. C. Young
Stanford Linear Accelerator Center, Stanford, California 94309, USA

P. R. Burchat, A. J. Edwards, S. A. Majewski, B. A. Petersen, C. Roat
Stanford University, Stanford, California 94305-4060, USA

M. Ahmed, S. Ahmed, M. S. Alam, J. A. Ernst, M. A. Saeed, F. R. Wappler, S. B. Zain
State University of New York, Albany, New York 12222, USA

W. Bugg, M. Krishnamurthy, S. M. Spanier
University of Tennessee, Knoxville, Tennessee 37996, USA

R. Eckmann, J. L. Ritchie, A. Satpathy, R. F. Schwitters
University of Texas at Austin, Austin, Texas 78712, USA

J. M. Izen, I. Kitayama, X. C. Lou, S. Ye
University of Texas at Dallas, Richardson, Texas 75083, USA

F. Bianchi, M. Bona, F. Gallo, D. Gamba
Università di Torino, Dipartimento di Fisica Sperimentale and INFN, I-10125 Torino, Italy

M. Bomben, L. Bosisio, C. Cartaro, F. Cossutti, G. Della Ricca, S. Dittongo, S. Grancagnolo, L. Lanceri,
L. Vitale
Università di Trieste, Dipartimento di Fisica and INFN, I-34127 Trieste, Italy

F. Martinez-Vidal
IFIC, Universitat de Valencia-CSIC, E-46071 Valencia, Spain

R. S. Panvini³
Vanderbilt University, Nashville, Tennessee 37235, USA

Sw. Banerjee, B. Bhuyan, C. M. Brown, D. Fortin, K. Hamano, R. Kowalewski, J. M. Roney, R. J. Sobie
University of Victoria, Victoria, British Columbia, Canada V8W 3P6

J. J. Back, P. F. Harrison, T. E. Latham, G. B. Mohanty
Department of Physics, University of Warwick, Coventry CV4 7AL, United Kingdom

H. R. Band, X. Chen, B. Cheng, S. Dasu, M. Datta, A. M. Eichenbaum, K. T. Flood, M. Graham,
J. J. Hollar, J. R. Johnson, P. E. Kutter, H. Li, R. Liu, B. Mellado, A. Mihalyi, Y. Pan, R. Prepost,
P. Tan, J. H. von Wimmersperg-Toeller, S. L. Wu, Z. Yu
University of Wisconsin, Madison, Wisconsin 53706, USA

H. Neal
Yale University, New Haven, Connecticut 06511, USA

³Deceased

1 Introduction

The decays $B \rightarrow K\ell^+\ell^-$ and $B \rightarrow K^*\ell^+\ell^-$, where $\ell^+\ell^-$ are the charged lepton pairs e^+e^- or $\mu^+\mu^-$ and K^* is the $K^*(892)$ meson, result from $b \rightarrow s$ flavor-changing neutral currents (FCNC). In the Standard Model (SM) of electroweak interactions, such $b \rightarrow s$ processes are forbidden in tree-level Feynman diagrams; they are allowed at lowest order through one-loop diagrams involving the emission and re-absorption of W bosons. Because the lowest order SM diagrams are loops of weakly interacting particles with virtual energies comparable to the electroweak scale, new flavor-changing interactions at the electroweak scale can introduce loop diagrams with comparable amplitudes. The SM predictions of the rates and kinematic distributions of FCNC decays can be significantly modified by a broad class of new physics models, such as a charged Higgs boson [1], topcolor [1], weak-scale supersymmetry [2,3], fourth-generation fermions [4], or leptoquarks [5].

In the SM, three amplitudes contribute at lowest order to the $b \rightarrow s\ell^+\ell^-$ process: a photon penguin, a Z penguin, and a W^+W^- box diagram (Figure 1). The magnitude of the photon penguin amplitude is well known experimentally from measurements of the rate of the FCNC decay $b \rightarrow s\gamma$ [6] and agrees well with SM predictions [7]. The latter two amplitudes are not well known and thus studies of $b \rightarrow s\ell^+\ell^-$ provide new information on FCNC processes. The SM decay rate of $b \rightarrow s\ell^+\ell^-$ is suppressed relative to other b decays, resulting in a predicted total branching fraction of $(4.2 \pm 0.7) \times 10^{-6}$ [3], in agreement with experiment [8].

The most abundant exclusive decays associated with the $b \rightarrow s\ell^+\ell^-$ transition, $B \rightarrow K\ell^+\ell^-$ and $B \rightarrow K^*\ell^+\ell^-$, are predicted to have branching fractions of 0.4×10^{-6} for $B \rightarrow K\ell^+\ell^-$ and about three times that for $B \rightarrow K^*\ell^+\ell^-$ [3,9–13], with a theoretical uncertainty of 30%. The theoretical uncertainty is predominantly due to the uncertainty in the prediction of semileptonic form factors, which model the rate that a $b \rightarrow s$ FCNC in a B decay results in a single $K^{(*)}$ meson. The partial widths of $B \rightarrow Ke^+e^-$ and $B \rightarrow K\mu^+\mu^-$ are expected to be identical, because of identical electroweak couplings of electrons and muons. The branching fractions of both $B \rightarrow K^*e^+e^-$ and $B \rightarrow K^*\mu^+\mu^-$, however, receive a contribution from a pole in the photon penguin amplitude at $q^2 = m_{\ell^+\ell^-}^2 \simeq 0$, and the enhancement in the electron mode is significantly larger due to its lower q^2 threshold. This phase space difference in the pole contribution is expected to reduce the ratio $\Gamma(B \rightarrow K^*\mu^+\mu^-)/\Gamma(B \rightarrow K^*e^+e^-)$ from unity to 0.752 [3]. Previous measurements

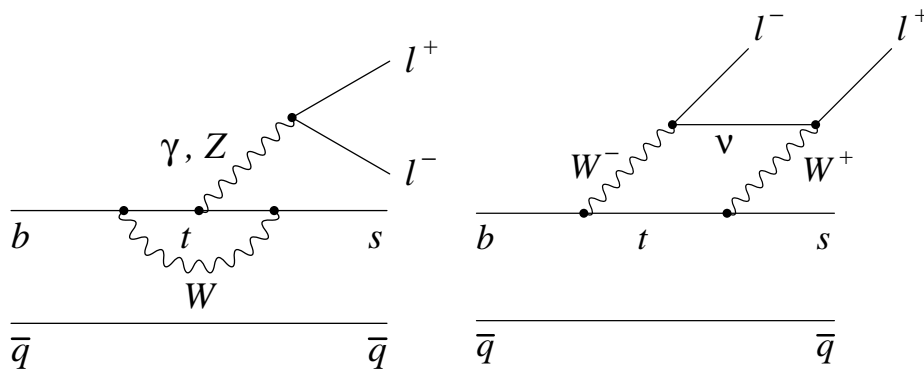


Figure 1: Examples of Standard Model diagrams for the decays $B \rightarrow K^{(*)}\ell^+\ell^-$. For the photon or Z penguin diagrams on the left, boson emission can occur on any of the b , t , s , or W lines.

of the exclusive decays are consistent with predictions [14–16]. In the absence of new physics contributions, improved precision in the exclusive branching fractions will improve experimental constraints of $B \rightarrow K^{(*)}$ form factors.

More precise SM tests can be obtained from rate asymmetries and kinematic distributions of the exclusive decay products. The direct CP asymmetries

$$A_{CP} = \frac{\Gamma(\bar{B} \rightarrow K^{(*)}\ell^+\ell^-) - \Gamma(B \rightarrow K^{(*)}\ell^+\ell^-)}{\Gamma(\bar{B} \rightarrow K^{(*)}\ell^+\ell^-) + \Gamma(B \rightarrow K^{(*)}\ell^+\ell^-)}$$

for these decays are expected to be very small in the SM, much less than 1% [17], whereas new physics at the electroweak scale could enhance A_{CP} to values of order one [18]. If one neglects the pole region ($q^2 < 0.1 \text{ GeV}^2/c^4$) of $B \rightarrow K^*e^+e^-$, in the SM the ratios

$$R_K = \mathcal{B}(B \rightarrow K\mu^+\mu^-)/\mathcal{B}(B \rightarrow Ke^+e^-),$$

$$R_{K^*} = \mathcal{B}(B \rightarrow K^*\mu^+\mu^-)/\mathcal{B}(B \rightarrow K^*e^+e^-)$$

are expected to be unity with high precision. However, this ratio could be enhanced by corrections of order 10% due to the presence of a supersymmetric neutral Higgs boson with large $\tan\beta$ (ratio of vacuum expectation values of the two Higgs doublets) [19]. The Feynman diagram of this process is shown in Figure 2. A large $\tan\beta$ would enhance the Higgs/squark coupling, and the Higgs decays to muons will be enhanced relative to decays to electrons because of the large ratio of Yukawa couplings m_μ^2/m_e^2 . A measurement of the relative abundance of electrons and muons in exclusive decays is therefore a probe of scalar penguin processes and complements the limits obtained from searches for the rare decay $B_s \rightarrow \mu^+\mu^-$ [20]. With sufficiently large samples of $B \rightarrow K^*\ell^+\ell^-$ events, angular asymmetries in the four-particle final state can also accurately gauge the relative phase and magnitude of the three contributing FCNC amplitudes [2, 3, 17].

2 Detector and Datasets

We analyze data collected with the *BABAR* detector at the PEP-II storage ring at the Stanford Linear Accelerator Center. The data sample comprises 208.0 fb^{-1} recorded on the $\Upsilon(4S)$ resonance,

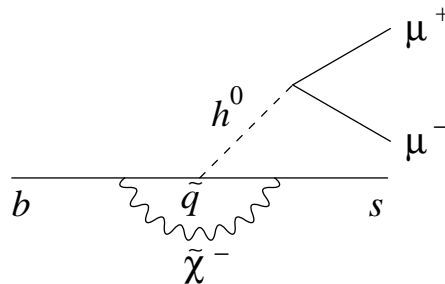


Figure 2: Feynman diagram of a Higgs penguin process which would enhance $b \rightarrow s\mu^+\mu^-$ relative to $b \rightarrow se^+e^-$.

yielding $(229.0 \pm 2.5) \times 10^6 B\bar{B}$ decays, and an off-resonance sample of 22.1 fb^{-1} used to study continuum background.

The *BABAR* detector is described in detail elsewhere [21]. The most important capabilities of the detector for this study are charged-particle tracking and momentum measurement, charged π/K separation, and lepton identification. Charged particle tracking is provided by a five-layer silicon vertex tracker (SVT) and a 40-layer drift chamber (DCH). The DIRC, a Cherenkov ring-imaging particle-identification system, is used (along with dE/dx measured in the trackers) to separate charged kaons and pions. Electrons are identified using an electromagnetic calorimeter (EMC), which comprises 6580 thallium-doped CsI crystals. These systems are mounted inside a 1.5 T solenoidal superconducting magnet. Muons are identified in an instrumented flux return (IFR), in which resistive plate chambers are interleaved with the iron plates of the magnet flux return.

Simulated samples of signal B decays, charmonium B decays, generic $B\bar{B}$ decays, and continuum $e^+e^- \rightarrow q\bar{q}$ (for $q = u, d, s, \text{ or } c$) events are used to compute selection efficiencies, optimize event selection, and estimate certain backgrounds, as described below. The simulation is based on GEANT4 [22] detector emulation software. The model for simulating signal B decays is a $b \rightarrow s\ell^+\ell^-$ matrix element calculation, which includes $\mathcal{O}(\alpha_s)$ and $\mathcal{O}(\Lambda_{\text{QCD}}/m_b)$ corrections [3], convolved with $B \rightarrow K^{(*)}$ form factors predicted by light-cone QCD sum rules [10].

3 Event Selection

We select events that include two oppositely charged lepton candidates (e^+e^- , $\mu^+\mu^-$), a kaon candidate (either K^\pm or K_S^0), and, for the $B \rightarrow K^*\ell^+\ell^-$ modes, a π^\pm candidate that, when combined with a kaon candidate, forms a K^* candidate. Electron (muon) candidates are identified by a likelihood (neural-net) based algorithm, and are required to have a minimum momentum $p > 0.3 \text{ GeV}/c$ ($p > 0.7 \text{ GeV}/c$) in the laboratory frame.

Bremsstrahlung photons from electrons are recovered by combining an electron candidate with up to one photon with $E_\gamma > 30 \text{ MeV}$. Recovered photons are restricted to an angular region in the laboratory frame of $(\theta_\gamma, \phi_\gamma) = (\theta_e \pm 35 \text{ mrad}, \phi_e \pm 50 \text{ mrad})$ around the initial electron direction (θ_e, ϕ_e) . Photon conversions and π^0 Dalitz decays are removed by vetoing all e^+e^- pairs with invariant mass less than $0.03 \text{ GeV}/c^2$, except in $B \rightarrow K^*e^+e^-$ modes, where we preserve acceptance at low invariant masses by retaining pairs that intersect inside the beam pipe.

Charged kaon candidates are tracks with dE/dx and DIRC Cherenkov angle consistent with the angle expected for a kaon. π^\pm candidates are tracks that do not satisfy the K^\pm selection. K_S^0 candidates are reconstructed from two oppositely charged tracks with an invariant mass (computed assuming they are $\pi^+\pi^-$) consistent with the K_S^0 mass and a common vertex displaced from the average interaction point by at least 1 mm.

True B signal decays produce narrow peaks in the distributions of two kinematic variables, which can be fitted to extract the signal and background yields. For a candidate system of B daughter particles with total momentum \mathbf{p}_B in the laboratory frame and energy E_B^* in the $\Upsilon(4S)$ center-of-mass (CM) frame, we define $m_{\text{ES}} = \sqrt{(s/2 + c^2\mathbf{p}_0 \cdot \mathbf{p}_B)^2/E_0^2 - c^2p_B^2}$ and $\Delta E = E_B^* - \sqrt{s}/2$, where E_0 and \mathbf{p}_0 are the energy and momentum of the $\Upsilon(4S)$ in the laboratory frame, and \sqrt{s} is the total CM energy of the e^+e^- beams. For signal events, the m_{ES} distribution peaks at the B meson mass with resolution $\sigma \approx 2.5 \text{ MeV}/c^2$, and the ΔE distribution peaks near zero, with a typical width $\sigma \approx 20 \text{ MeV}$. In $B \rightarrow K\ell^+\ell^-$ channels, we perform a two-dimensional unbinned maximum-likelihood fit to the distribution of m_{ES} and ΔE in the region $m_{\text{ES}} > 5.2 \text{ GeV}/c^2$ and

$|\Delta E| < 0.25$ GeV. In $B \rightarrow K^* \ell^+ \ell^-$ decays, we perform a three-dimensional fit to m_{ES} , ΔE , in the same regions as for $B \rightarrow K \ell^+ \ell^-$, and in addition we include in the fit the kaon-pion invariant mass for the region $0.7 < m_{K\pi} < 1.1$ GeV/ c^2 .

Backgrounds arise from four main sources: (1) random combinations of particles from $q\bar{q}$ events produced in the continuum, (2) random combinations of particles from $\Upsilon(4S) \rightarrow B\bar{B}$ decays, (3) B decays to $s\ell^+\ell^-$ final states other than the signal mode (“crossfeed”) and (4) B decays to topologies similar to the signal modes. The first two (“combinatorial”) backgrounds typically arise from pairs of semileptonic decays of D or B mesons and produce distributions in m_{ES} and ΔE which are broadly distributed compared to the signal. The third source has m_{ES} similar to signal, but the peak of the ΔE distribution is significantly offset from the signal due to the addition of a random particle (“feed-up”) or omission of one of the B daughters (“feed-down”). The last source arises from modes such as $B \rightarrow J/\psi K^{(*)}$ (with $J/\psi \rightarrow \ell^+\ell^-$) or $B \rightarrow K^{(*)}\pi\pi$ (with pions misidentified as muons), which have shapes similar to the signal. All selection criteria are optimized with simulated data or with data samples outside the region of the maximum-likelihood fit.

3.1 Combinatorial backgrounds

We suppress combinatorial background from continuum processes using a Fisher discriminant [23], which is a linear combination of variables with coefficients optimized to distinguish between signal and background. The variables used in the Fisher discriminant are the following kinematic quantities computed in the CM frame: (1) the ratio of second- to zeroth-order Fox-Wolfram moments [24] for the event, computed using all charged tracks and neutral energy clusters; (2) the angle between the thrust axis of the B candidate and that of the remaining particles in the event; (3) the production angle θ_B of the B candidate with respect to the beam axis; and (4) the masses of $K\ell$ pairs with the same charge correlation as a semileptonic D decay. The first three variables exploit the differences in event shapes between the jet-like topology of light quark pair production and the spherical shape of $\Upsilon(4S) \rightarrow B\bar{B}$ production. The fourth variable discriminates between D meson decays, which have $K\ell$ mass distributed below the D mass, and signal decays, which have a broad distribution in $K\ell$ mass.

We suppress combinatorial backgrounds from $B\bar{B}$ events using a likelihood function constructed from (1) the missing energy of the event, computed from all charged tracks and neutral energy clusters; (2) the vertex fit probability of all tracks from the B candidate; (3) the vertex fit probability of the two leptons; and (4) the angle θ_B . Missing energy provides the strongest suppression of combinatorial $B\bar{B}$ background events, which typically contain neutrinos from two semileptonic B decays.

The parameters of the Fisher discriminant and the likelihood function are determined separately for each of the eight signal decay modes. The selection criteria for the background suppression variables are optimized simultaneously, and are chosen to minimize signal yield statistical uncertainties in each mode. The efficiencies of the Fisher and likelihood requirements are validated by comparing the efficiencies in data and in simulation using the $B \rightarrow J/\psi K^{(*)}$ control sample.

3.2 Peaking backgrounds

The largest backgrounds that peak in m_{ES} and ΔE are B decays to charmonium: $B \rightarrow J/\psi K^{(*)}$ (with $J/\psi \rightarrow \ell^+\ell^-$) and $B \rightarrow \psi(2S)K^{(*)}$ (with $\psi(2S) \rightarrow \ell^+\ell^-$). We exclude dilepton pairs consistent with the J/ψ mass ($2.90 < m_{e^+e^-} < 3.20$ GeV/ c^2 and $3.00 < m_{\mu^+\mu^-} < 3.20$ GeV/ c^2) or with the $\psi(2S)$ mass ($3.60 < m_{\ell^+\ell^-} < 3.75$ GeV/ c^2). This veto is applied to $m_{e^+e^-}$ both with and

without the inclusion of bremsstrahlung photon recovery. When a lepton radiates or is mismeasured, $m_{\ell^+\ell^-}$ can shift away from the charmonium mass, while ΔE shifts in a correlated manner. The veto region is extended in the $(m_{\ell^+\ell^-}, \Delta E)$ plane to account for this correlation (Figure 3), removing nearly all charmonium events and simplifying the description of the background in the fit. Because the charmonium events removed by these vetoes are so similar to signal events, these modes provide large control samples (about 13700 events of $B \rightarrow J/\psi K^{(*)}$ and 1000 events of $B \rightarrow \psi(2S)K^{(*)}$ in all) for studying signal shapes, selection efficiencies, and systematic uncertainties. After the vetoes on $B \rightarrow J/\psi K^{(*)}$ and $B \rightarrow \psi(2S)K^{(*)}$ decays, the remaining peaking background from these processes is estimated from simulation to be 0.0–1.6 events, depending on the decay mode.

In the muon modes, the pion misidentification rate is significant ($\sim 2\%$), leading to additional peaking backgrounds from the decay $B^- \rightarrow D^0\pi^-$ with $D^0 \rightarrow K^-\pi^+$ or $D^0 \rightarrow K^{*-}\pi^+$, or from $\bar{B}^0 \rightarrow D^+\pi^-$ with $D^+ \rightarrow \bar{K}^{*0}\pi^+$ (and their charge conjugates [25]). These events are suppressed by vetoing events where the $K^{(*)}\mu$ mass is consistent with a hadronic D decay. The remaining background from the charmless decays $B \rightarrow K^{(*)}\pi\pi$, $B \rightarrow K^{(*)}K\pi$, and $B \rightarrow K^{(*)}KK$ is estimated from data. We select control samples of $B \rightarrow K^{(*)}h\mu$ events with the same requirements as signal events, except that muon particle identification is no longer required for the hadron candidate h and hadron identification requirements for pions and kaons are used instead. This results in a sample of predominantly hadronic B decays. Each event is given a weight corresponding to the muon misidentification rate for the hadron divided by its hadron identification efficiency, and the number of peaking background events from hadronic B decays is extracted from the weighted m_{ES} distribution through a maximum-likelihood fit similar to that used to extract a signal. The control sample calculations result in an estimate of 0.4–2.3 background events per decay channel for $B \rightarrow K^{(*)}\mu^+\mu^-$ modes.

Finally, there is a peaking contribution to the electron modes from the rare decays $B \rightarrow K^*\gamma$ (with photon conversion in the detector), $B \rightarrow K^{(*)}\pi^0$, and $B \rightarrow K^{(*)}\eta$ (with a π^0 or η Dalitz decay to $e^+e^-\gamma$). The sum of these backgrounds is estimated from simulation to be 0.0–1.4 per decay channel for the $B \rightarrow K^{(*)}e^+e^-$ modes.

The number of peaking background events from all sources is shown in Table 1 for the individual decay modes. The peaking backgrounds in the modes with electrons are dominated by processes with real electrons, and the uncertainties are dominated by simulation statistics. The peaking backgrounds for modes with muons are dominated by hadrons misidentified as muons; the dominant uncertainty here is systematic and originates from the unknown K/π composition of the contributing hadrons.

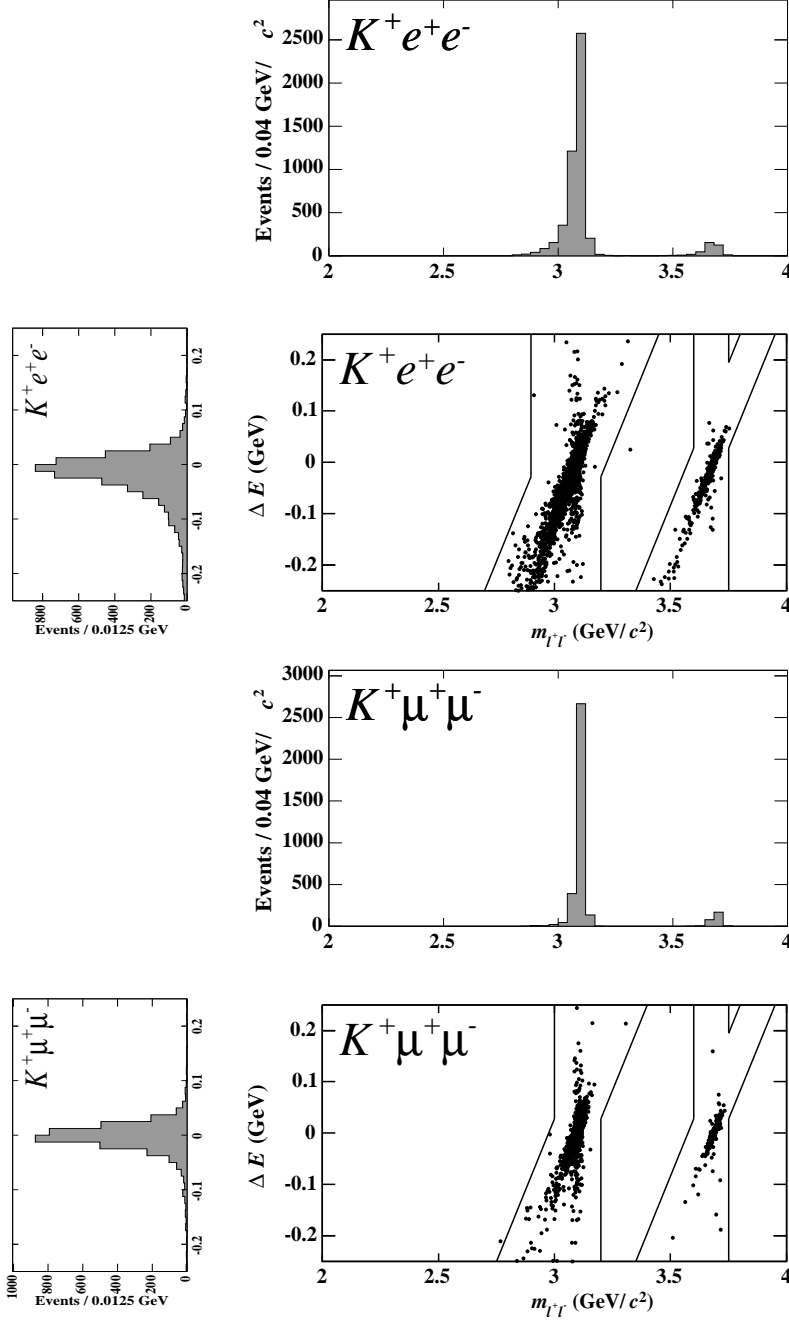


Figure 3: Charmonium veto regions in the $B^+ \rightarrow K^+e^+e^-$ (above) and $B^+ \rightarrow K^+\mu^+\mu^-$ (below) channels. The points are simulated J/ψ and $\psi(2S)$ events, with abundance equal to the mean number expected in 208 fb^{-1} . The projections onto $m_{\ell^+\ell^-}$ and ΔE are shown above and at left, which indicate the high density of points at $(m_{\ell^+\ell^-}, \Delta E) = (m_\psi, 0.0)$. The vertical band corresponds to events where the J/ψ ($\psi(2S)$) and K^+ come from different B decays; the diagonal band corresponds to events with mismeasured leptons.

Table 1: Mean expected peaking backgrounds in 208 fb^{-1} , for the individual $K^{(*)}\ell^+\ell^-$ decay modes after applying all selection requirements.

Decay mode	Events
$B^+ \rightarrow K^+ e^+ e^-$	0.7 ± 0.2
$B^+ \rightarrow K^+ \mu^+ \mu^-$	2.3 ± 0.5
$B^0 \rightarrow K_s^0 e^+ e^-$	0.01 ± 0.01
$B^0 \rightarrow K_s^0 \mu^+ \mu^-$	0.4 ± 0.1
$B^0 \rightarrow K^{*0} e^+ e^-$	3.0 ± 0.6
$B^0 \rightarrow K^{*0} \mu^+ \mu^-$	1.4 ± 0.8
$B^+ \rightarrow K^{*+} e^+ e^-$	0.9 ± 0.2
$B^+ \rightarrow K^{*+} \mu^+ \mu^-$	0.6 ± 0.3

4 Fits

For $B \rightarrow K\ell^+\ell^-$, a two-dimensional fit to m_{ES} and ΔE is performed. For $B \rightarrow K^*\ell^+\ell^-$, the mass of the K^* is added as a third fit variable. The signal shapes are parameterized with separate Crystal Ball functions [26] for m_{ES} and ΔE . Both the m_{ES} and ΔE shape include a radiative tail, which accounts for the effects of bremsstrahlung of the electrons in the *BABAR* detector. The m_{ES} shape parameters are additionally assumed to have ΔE dependence $c_0 + c_2(\Delta E)^2$; the variation of the m_{ES} width due to the quadratic term is typically a few percent of c_0 . All signal shape parameters are fixed from the signal simulation, except for the mean and width parameters in m_{ES} and ΔE , which are fixed to values from charmonium data control samples (for the m_{ES} width, c_0 is fixed from charmonium data and c_2 is fixed from signal simulation). In the $B \rightarrow K^*\ell^+\ell^-$ channels, the K^* is fitted with a relativistic Breit-Wigner line shape. Adding the mass of the K^* to the likelihood fit increases the precision of the $B \rightarrow K^*\ell^+\ell^-$ branching fraction measurement by approximately 10%.

The background is modeled as the sum of three or four terms: (1) a combinatorial background shape with floating normalization, written as the product of an ARGUS function [27] in m_{ES} , a linear term in ΔE , and the product of $\sqrt{m_{K\pi} - m_K - m_\pi}$ and a quadratic function of $m_{K\pi}$ for the K^* modes; (2) a peaking background contribution, with the same shape as the signal, but with normalization fixed to estimates of the mean peaking backgrounds (see Table 1); and (3) terms with floating normalization to describe (a) background in $B \rightarrow K\ell^+\ell^-$ ($B \rightarrow K^*\ell^+\ell^-$) from $B \rightarrow K^*\ell^+\ell^-$ ($B \rightarrow K^*\pi\ell^+\ell^-$) events with a lost pion, and (b) background in $B \rightarrow K^*\ell^+\ell^-$ from $B \rightarrow K\ell^+\ell^-$ events with a randomly added pion. In the K^* modes, we allow an additional background (4) that uses our combinatorial shape in m_{ES} and ΔE , but peaks in $m_{K\pi}$ at the K^* mass. The yield of this term is fixed to $(5 \pm 5)\%$ of the total combinatorial background, as determined from simulation. Because the normalizations for terms (1) and (3) are floating, as are the combinatorial background shape parameters, much of the uncertainty in the background is propagated into the statistical uncertainty on the signal yield obtained from the fit.

The direct CP asymmetry A_{CP} is also extracted from the fit to the modes $B^+ \rightarrow K^+\ell^+\ell^-$ and $B \rightarrow K^*\ell^+\ell^-$, where the b flavor of signal candidates can be inferred directly from the charges of the final state $K^{(*)}$ hadrons. It is not possible at this time to measure A_{CP} in the mode $B^0 \rightarrow K_S^0\ell^+\ell^-$, as the signal statistics are small and the b flavor can only be inferred indirectly from properties of the other B meson. The CP asymmetry of the combinatorial background is allowed to float in the fit, while the asymmetries of the peaking background and crossfeed background are fixed to 0 and varied from -1 to 1 to evaluate the systematic uncertainty associated with these components.

5 Systematic Uncertainties

Table 2 lists the relative systematic uncertainties on the efficiency for each mode. The sources of uncertainty considered are: charged-particle tracking (0.8% per lepton, 1.4% per charged hadron), charged-particle identification (0.5% per electron pair, 1.3% per muon pair, 0.2% per pion, 0.6% per kaon), the continuum suppression cut (0.3%–2.2%, depending on the mode), the $B\bar{B}$ suppression cut (0.6%–2.1%), K_S^0 selection (0.9%), signal simulation statistics (0.4%–0.7%), and the number of $B\bar{B}$ events (1.1%). The uncertainty in the signal efficiency due to model dependence of form factors is evaluated for each mode to be the full range of variation from a set of models. The models considered are based on QCD sum rules [9], light-cone QCD sum rules [10], and lattice QCD [11]. The model dependence enters through the variation in q^2 distributions; since the selection efficiency is

not highly sensitive to this distribution the efficiency varies by only 4%–7%. For branching fraction measurements which combine modes, the systematic uncertainty is an appropriately weighted sum of correlated and uncorrelated sources from the contributing modes. The total systematic uncertainty in the signal efficiency introduces a systematic uncertainty $\Delta\mathcal{B}_{\text{eff}}$ in the measured branching fraction.

Table 2: Systematic uncertainties of selection efficiency (in %) considered for $K^{(*)}\ell^+\ell^-$ decays.

Source	$K^+e^+e^-$	$K^+\mu^+\mu^-$	$K_S e^+e^-$	$K_S \mu^+\mu^-$	$K^{*0}e^+e^-$	$K^{*0}\mu^+\mu^-$	$K^{*+}e^+e^-$	$K^{*+}\mu^+\mu^-$
Trk eff. (e, μ)	± 1.6	± 1.6	± 1.6	± 1.6	± 1.6	± 1.6	± 1.6	± 1.6
Electron ID	± 0.5	-	± 0.5	-	± 0.5	-	± 0.5	-
Muon ID	-	± 1.3	-	± 1.3	-	± 1.3	-	± 1.3
Kaon ID	± 0.6	± 0.6	-	-	± 0.6	± 0.6	-	-
Pion ID	-	-	-	-	± 0.2	± 0.2	± 0.2	± 0.2
Trk eff. (K, π)	± 1.4	± 1.4	± 2.8	± 2.8	± 2.8	± 2.8	± 4.2	± 4.2
K_S eff.	-	-	± 0.9	± 0.9	-	-	± 0.9	± 0.9
$B\bar{B}$ counting	± 1.1	± 1.1	± 1.1	± 1.1	± 1.1	± 1.1	± 1.1	± 1.1
Fisher	± 0.3	± 0.5	± 0.6	± 1.1	± 0.6	± 1.0	± 1.1	± 2.2
$B\bar{B}$ likelihood	± 0.6	± 0.6	± 0.9	± 0.9	± 0.9	± 0.9	± 1.7	± 2.1
Model dep.	± 4.0	± 4.0	± 4.0	± 4.0	± 4.0	± 7.0	± 4.0	± 7.0
MC statistics	± 0.4	± 0.5	± 0.4	± 0.5	± 0.5	± 0.6	± 0.5	± 0.7
Total	± 5.2	± 5.4	± 6.3	± 6.4	± 6.2	± 8.6	± 7.5	± 9.8

Systematic uncertainties on the signal yields obtained from the maximum-likelihood fit arise from three sources: uncertainties in the parameters describing the signal shapes, uncertainties in the combinatorial background shape, and uncertainties in the peaking backgrounds. The uncertainties in the means and widths of the signal shapes are obtained by comparing data and simulated data in charmonium control samples. For modes with electrons, we also vary the fraction of signal events in the tail of the ΔE distribution. To evaluate the uncertainty due to the background shape, we reevaluate the fit yields with three different parameterizations: (1) an exponential shape for ΔE , (2) a quadratic shape for ΔE , and (3) an m_{ES} ARGUS slope parameter ζ [27], which is linearly correlated with ΔE . The total systematic uncertainty in the fitted signal yield introduces a systematic uncertainty $\Delta\mathcal{B}_{\text{fit}}$ in the measured branching fraction.

As cross checks, we also test our fit method by measuring the branching fractions and A_{CP} of the J/ψ $K^{(*)}$ and $\psi(2S)$ $K^{(*)}$ final states using the vetoed charmonium events. The measured branching fractions are in good agreement with the 2004 world average [28] and the recent *BABAR* measurement [29]. The direct CP asymmetries A_{CP} are all consistent with zero. We also analyze $K^{(*)}e\mu$ samples and obtain signal yields consistent with zero.

6 Results

The results for the fits to the individual decay modes are shown in Table 3. Branching fraction uncertainties are predominantly statistical, with total systematic uncertainties of about 10% in each decay mode.

To combine the results from the individual modes into the total $B \rightarrow K\ell^+\ell^-$ and $B \rightarrow K^*\ell^+\ell^-$ branching fractions, we perform a maximum-likelihood fit where the event yields in all of the modes, after being corrected for selection efficiency and $K^{(*)}$ branching fractions, are constrained to the

Table 3: Results from fits to the individual $K^{(*)}\ell^+\ell^-$ decay modes. The columns from left are: decay mode, fitted signal yield, signal efficiency, systematic error on the selection efficiency, systematic error from the fit, the resulting branching fraction (with statistical and systematic errors), and the significance of the signal (including systematic errors).

Mode	Signal yield	Efficiency (%)	$\Delta\mathcal{B}_{\text{eff}}$ (10^{-6})	$\Delta\mathcal{B}_{\text{fit}}$ (10^{-6})	\mathcal{B} (10^{-6})	Significance (σ)
$B^+ \rightarrow K^+e^+e^-$	$25.9^{+7.4}_{-6.5}$	26.4	± 0.02	± 0.02	$0.43^{+0.12}_{-0.11} \pm 0.03$	5.3
$B^+ \rightarrow K^+\mu^+\mu^-$	$10.9^{+5.1}_{-4.3}$	15.2	± 0.02	± 0.04	$0.31^{+0.15}_{-0.12} \pm 0.04$	3.0
$B^0 \rightarrow K^0e^+e^-$	$2.4^{+2.8}_{-2.0}$	22.6	± 0.01	± 0.01	$0.14^{+0.16}_{-0.11} \pm 0.02$	1.2
$B^0 \rightarrow K^0\mu^+\mu^-$	$6.3^{+3.6}_{-2.8}$	13.3	± 0.04	± 0.03	$0.60^{+0.34}_{-0.27} \pm 0.05$	2.8
$B^0 \rightarrow K^{*0}e^+e^-$	$29.4^{+9.5}_{-8.4}$	18.7	± 0.06	± 0.10	$1.03^{+0.33}_{-0.29} \pm 0.12$	4.4
$B^0 \rightarrow K^{*0}\mu^+\mu^-$	$15.9^{+7.0}_{-5.9}$	11.7	± 0.08	± 0.11	$0.89^{+0.39}_{-0.33} \pm 0.14$	3.3
$B^+ \rightarrow K^{*+}e^+e^-$	$6.2^{+7.0}_{-5.6}$	15.4	± 0.07	± 0.60	$0.77^{+0.87}_{-0.70} \pm 0.60$	1.0
$B^+ \rightarrow K^{*+}\mu^+\mu^-$	$4.7^{+4.6}_{-3.4}$	9.0	± 0.10	± 0.13	$1.00^{+0.96}_{-0.71} \pm 0.16$	1.6

same value. In this fit we constrain the production rates of charged and neutral B meson pairs in the $\Upsilon(4S)$ decay to be the same. We also constrain the total width ratio $\Gamma(B^0)/\Gamma(B^+)$ to the world average B meson lifetime ratio $\tau_+/\tau_0 = 1.086 \pm 0.017$ [28]; all branching fractions from combined fits are expressed in terms of the B^0 total width. In $B \rightarrow K^*\ell^+\ell^-$ we perform the fit with the pole region included, adding the constraint:

$$\Gamma(B \rightarrow K^*\mu^+\mu^-)/\Gamma(B \rightarrow K^*e^+e^-) = 0.752.$$

As described in Section 1, this originates from the enhanced contribution in $B \rightarrow K^*e^+e^-$ from the photon penguin amplitude near $q^2 = 0$. The branching fraction for this combined fit is expressed in terms of the $B^0 \rightarrow K^{*0}\mu^+\mu^-$ channel. We also perform combined fits to the electron and muon channels separately. Table 4 summarizes the results for the combined branching fractions. The combined significance of the signal, including statistical and systematic uncertainties, is 6.6σ and 5.7σ for the $B \rightarrow K\ell^+\ell^-$ and $B \rightarrow K^*\ell^+\ell^-$ modes, respectively.

The combined fits to $B \rightarrow K\ell^+\ell^-$ and $B \rightarrow K^*\ell^+\ell^-$ are shown in Figures 4 and 5. They correspond to the branching fraction measurements of

$$\mathcal{B}(B \rightarrow K\ell^+\ell^-) = (0.34^{+0.07}_{-0.07} \pm 0.03) \times 10^{-6}$$

$$\mathcal{B}(B \rightarrow K^*\ell^+\ell^-) = (0.78^{+0.19}_{-0.17} \pm 0.12) \times 10^{-6}$$

where the first error is statistical and the second is systematic. The satellite peak in the ΔE distribution at -0.15 GeV for the $B \rightarrow K\ell^+\ell^-$ fit arises from the feed-down component of the fit. Examination of events in this region confirms that the addition of a charged or neutral pion results in candidates consistent with $B \rightarrow K^*\ell^+\ell^-$ signal. The effect of such events on the $B \rightarrow K\ell^+\ell^-$ signal yield has been studied with fits to simulated samples, and the associated bias to the signal yield is negligible.

For the combined modes we measure the direct CP asymmetries

$$A_{CP}(B^+ \rightarrow K^+\ell^+\ell^-) = 0.08 \pm 0.22 \pm 0.11$$

Table 4: Results from fits to the combined $K^{(*)}\ell^+\ell^-$ decay modes. The columns from left are: decay mode, fitted signal yield, systematic error on the selection efficiency, systematic error on the branching fraction introduced by the systematic error on the fitted signal yield, the resulting branching fraction (with statistical and systematic errors), and the significance of the signal (including systematic errors).

Mode	Signal yield	$\Delta\mathcal{B}_{\text{eff}}$ (10^{-6})	$\Delta\mathcal{B}_{\text{fit}}$ (10^{-6})	\mathcal{B} (10^{-6})	Significance (σ)
$B \rightarrow Ke^+e^-$	$27.9^{+7.7}_{-6.9}$	± 0.02	± 0.01	$0.33^{+0.09}_{-0.08} \pm 0.02$	5.3
$B \rightarrow K\mu^+\mu^-$	$17.1^{+6.1}_{-5.3}$	± 0.02	± 0.03	$0.35^{+0.13}_{-0.11} \pm 0.03$	3.8
$B^+ \rightarrow K^+\ell^+\ell^-$	$36.7^{+8.8}_{-8.0}$	± 0.02	± 0.02	$0.38^{+0.09}_{-0.08} \pm 0.03$	6.2
$B^0 \rightarrow K^0\ell^+\ell^-$	$8.2^{+4.4}_{-3.6}$	± 0.02	± 0.02	$0.29^{+0.16}_{-0.13} \pm 0.03$	2.8
$B \rightarrow K\ell^+\ell^-$	$45.0^{+9.7}_{-8.9}$	± 0.02	± 0.02	$0.34^{+0.07}_{-0.07} \pm 0.03$	6.6
$B \rightarrow K^*e^+e^-$	$36.1^{+11.2}_{-10.0}$	± 0.06	± 0.13	$0.97^{+0.30}_{-0.27} \pm 0.15$	4.5
$B \rightarrow K^*\mu^+\mu^-$	$20.7^{+8.1}_{-7.0}$	± 0.08	± 0.11	$0.90^{+0.35}_{-0.30} \pm 0.13$	3.5
$B^0 \rightarrow K^{*0}\ell^+\ell^-$	$45.2^{+11.6}_{-10.5}$	± 0.06	± 0.09	$0.81^{+0.21}_{-0.19} \pm 0.10$	5.4
$B^+ \rightarrow K^{*+}\ell^+\ell^-$	$11.4^{+8.0}_{-6.7}$	± 0.06	± 0.21	$0.74^{+0.52}_{-0.43} \pm 0.22$	1.5
$B \rightarrow K^*\ell^+\ell^-$	$56.8^{+13.6}_{-12.4}$	± 0.05	± 0.10	$0.78^{+0.19}_{-0.17} \pm 0.12$	5.7

$$A_{CP}(B \rightarrow K^*\ell^+\ell^-) = -0.03 \pm 0.23 \pm 0.12$$

where the systematic uncertainty is dominated by the unknown asymmetry in the peaking backgrounds.

Table 4 also contains the results from independent fits to the muon and electron channels, with no constraint enforced on the ratio of the two. From these fits we find the ratio of muon to electron branching fractions over the full range of q^2 to be

$$R_K = 1.06 \pm 0.48 \pm 0.05$$

$$R_{K^*} = 0.93 \pm 0.46 \pm 0.06$$

where these are expected in the Standard Model to be 1.00 and 0.75, respectively, with small theoretical uncertainties.

We also perform the fit to the $B \rightarrow K^*\ell^+\ell^-$ channels with the pole region ($q^2 < 0.1 \text{ GeV}^2/c^4$) excluded, which modifies the Standard Model constraint on the ratio of branching fractions from 0.752 to 1. With the pole region removed, we obtain

$$\begin{aligned}
\mathcal{B}(B \rightarrow K^*e^+e^-, q^2 > 0.1 \text{ GeV}^2/c^4) &= (0.65^{+0.24}_{-0.21} \pm 0.12) \times 10^{-6} \\
\mathcal{B}(B \rightarrow K^*\mu^+\mu^-, q^2 > 0.1 \text{ GeV}^2/c^4) &= (0.89^{+0.35}_{-0.30} \pm 0.13) \times 10^{-6} \\
\mathcal{B}(B \rightarrow K^*\ell^+\ell^-, q^2 > 0.1 \text{ GeV}^2/c^4) &= (0.74^{+0.20}_{-0.18} \pm 0.12) \times 10^{-6}
\end{aligned} \tag{1}$$

From the fits to the $B \rightarrow K^*\ell^+\ell^-$ mode above the pole region, we find the ratio of muon to electron branching fractions

$$R_{K^*}(q^2 > 0.1 \text{ GeV}^2/c^4) = 1.37^{+0.74}_{-0.74} \pm 0.11,$$

which is expected to be 1.00 in the Standard Model.

The measured $B \rightarrow K^*\ell^+\ell^-$ branching fraction is consistent with the previously published *BABAR* result [14] measured with 113 fb^{-1} , $\mathcal{B}(B \rightarrow K^*\ell^+\ell^-) = (0.88_{-0.29}^{+0.33} \pm 0.10) \times 10^{-6}$. The $B \rightarrow K\ell^+\ell^-$ branching fraction is somewhat lower than the previous published *BABAR* result of $\mathcal{B}(B \rightarrow K\ell^+\ell^-) = (0.65_{-0.13}^{+0.14} \pm 0.04) \times 10^{-6}$ [14]. Including correlations between events selected, the significance of this difference is equivalent to 2.2σ . The ratios $R_{K^{(*)}}$ of muon to electron branching fractions are also consistent with the previously published values.

As a cross check, we have also examined the $m_{\ell\ell}$ distribution of candidate events in the signal region. Of particular interest would be any evidence for a large excess in the $m_{\ell\ell}$ spectrum near the lower boundaries of the veto regions, which could indicate J/ψ or $\psi(2S)$ events escaping the veto. The $m_{\ell\ell}$ spectrum, shown in Figure 6, exhibits no evidence for such an enhancement. The data points cover the full allowed region in $m_{\ell\ell}$, including the pole region in $B \rightarrow K^*\ell^+\ell^-$.

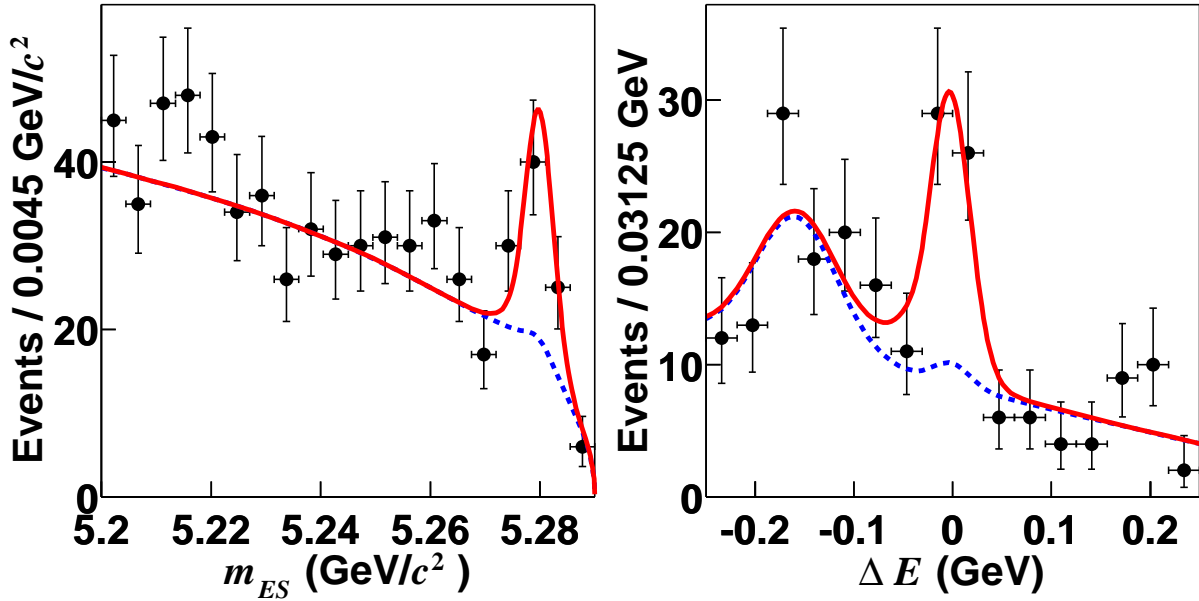


Figure 4: Distributions of the fit variables in $K\ell^+\ell^-$ data (points), compared with projections of the combined fit (curves): (left) m_{ES} distribution after requiring $-0.11 < \Delta E < 0.05$ GeV and (right) ΔE distribution after requiring $|m_{ES} - m_B| < 6.6$ MeV/c^2 . The solid curve is the sum of all fit components, including signal; the dashed curve is the sum of all background components.

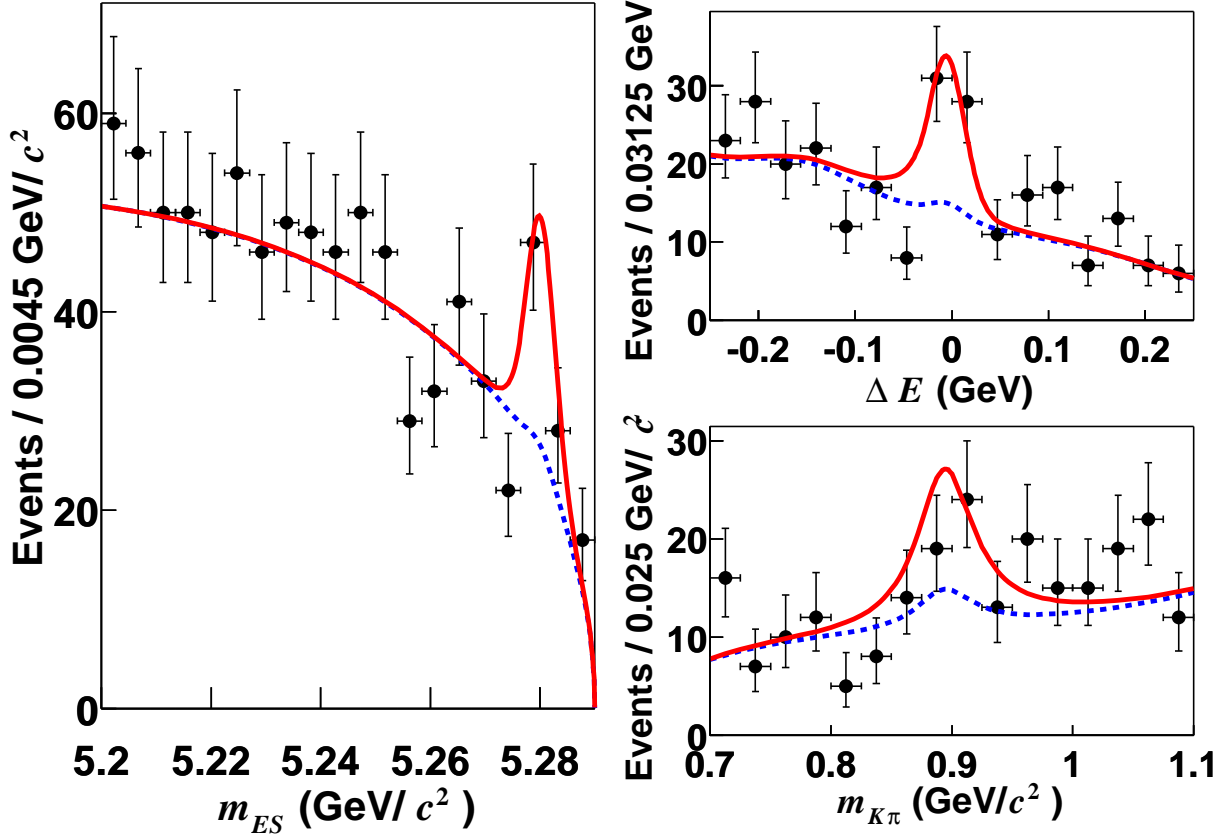


Figure 5: Distributions of the fit variables in $K^*\ell^+\ell^-$ data (points), compared with projections of the combined fit (curves): (left) m_{ES} after requiring $-0.11 < \Delta E < 0.05$ GeV and $0.817 < m_{K\pi} < 0.967$ GeV/c^2 , (upper right) ΔE after requiring $|m_{ES} - m_B| < 6.6$ MeV/c^2 , $0.817 < m_{K\pi} < 0.967$ GeV/c^2 , and (lower right) $m_{K\pi}$ after requiring $|m_{ES} - m_B| < 6.6$ MeV/c^2 and $-0.11 < \Delta E < 0.05$ GeV. The solid curve is the sum of all fit components, including signal; the dashed curve is the sum of all background components.

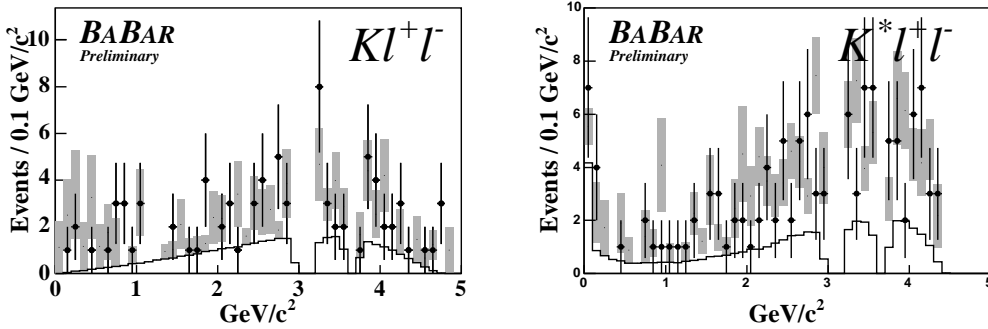


Figure 6: Distribution of $m_{\ell\ell}$ for candidates in the signal region for $B \rightarrow K\ell^+\ell^-$ (left) and $B \rightarrow K^*\ell^+\ell^-$ (right). The points are data. The dark gray bars are the total expectation from the sum of simulated signal and backgrounds, where the width of the bars reflects the uncertainty due to simulation statistics. The white histogram shows the signal subset of the total.

Figure 7 summarizes the experimental measurements (points) and their theoretical predictions (boxes). The measurements are in general agreement with the range of rates predicted by the form factor calculations in Ref. [3]. The measured $B^+ \rightarrow K^+\ell^+\ell^-$ branching fraction is significantly lower than the range estimated in [13].

7 Summary

We have measured the branching fractions and direct CP asymmetries A_{CP} of the rare FCNC decays $B \rightarrow K\ell^+\ell^-$ and $B \rightarrow K^*\ell^+\ell^-$. We find the (lepton-flavor-averaged, B -charge-averaged) branching fractions

$$\begin{aligned} \mathcal{B}(B \rightarrow K\ell^+\ell^-) &= (0.34 \pm 0.07 \pm 0.03) \times 10^{-6} \\ \mathcal{B}(B \rightarrow K^*\ell^+\ell^-) &= (0.78_{-0.17}^{+0.19} \pm 0.12) \times 10^{-6}, \end{aligned}$$

consistent with the Standard Model predictions for these modes. We find $A_{CP}(B^+ \rightarrow K^+\ell^+\ell^-)$ and $A_{CP}(B \rightarrow K^*\ell^+\ell^-)$ consistent with zero, to a precision of 25%. We have also measured the ratios of the branching fractions of muon pairs to that of electron pairs; these are also consistent with the Standard Model to a precision of 50%. All of the measurements are statistically limited.

8 Acknowledgments

We are grateful for the extraordinary contributions of our PEP-II colleagues in achieving the excellent luminosity and machine conditions that have made this work possible. The success of this project also relies critically on the expertise and dedication of the computing organizations that support *BABAR*. The collaborating institutions wish to thank SLAC for its support and the kind hospitality extended to them. This work is supported by the US Department of Energy and National Science Foundation, the Natural Sciences and Engineering Research Council (Canada), Institute of High Energy Physics (China), the Commissariat à l’Energie Atomique and Institut National de Physique Nucléaire et de Physique des Particules (France), the Bundesministerium für

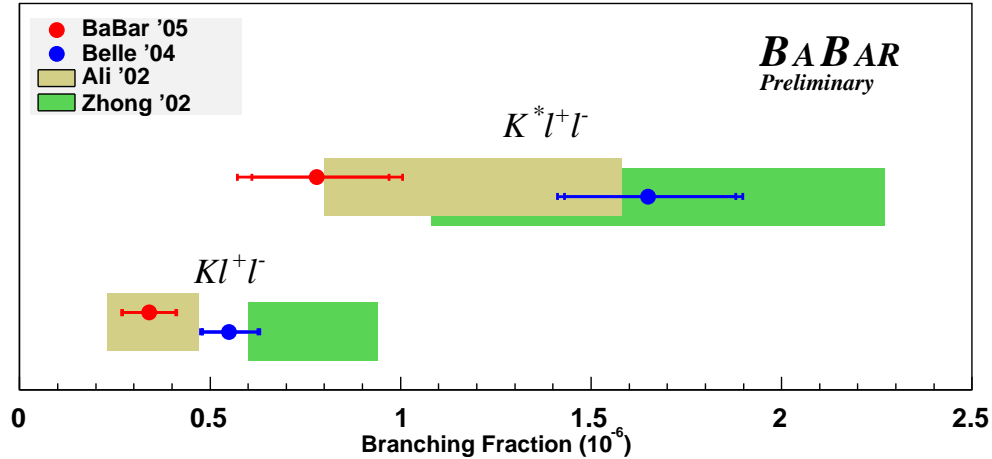


Figure 7: Experimental measurements (points) and theoretical predictions (boxes) for $K^{(*)}\ell^+\ell^-$ branching fractions. Red points are the results of this analysis, and the blue points are the preliminary results of [16]. Error bars on the points indicate statistical and total uncertainties; the width of the boxes indicate the estimated precision of the predictions [3, 13].

Bildung und Forschung and Deutsche Forschungsgemeinschaft (Germany), the Istituto Nazionale di Fisica Nucleare (Italy), the Foundation for Fundamental Research on Matter (The Netherlands), the Research Council of Norway, the Ministry of Science and Technology of the Russian Federation, and the Particle Physics and Astronomy Research Council (United Kingdom). Individuals have received support from CONACyT (Mexico), the A. P. Sloan Foundation, the Research Corporation, and the Alexander von Humboldt Foundation.

References

- [1] G. Burdman, Phys. Rev. D **52**, 6400 (1995).
- [2] J.L. Hewett and J.D. Wells, Phys. Rev. D **55**, 5549 (1997).
- [3] A. Ali *et al.*, Phys. Rev. D **66**, 034002 (2002).
- [4] G. Eilam, J. L. Hewett, and T. G. Rizzo, Phys. Rev. D **34**, 2773 (1986); T. M. Aliev, A. Ozpineci, and M. Savci, Eur. Phys. J. C **29**, 265 (2003).
- [5] S. Davidson, D. C. Bailey, and B. A. Campbell, Z. Phys. C **61**, 613 (1994).
- [6] Heavy Flavor Averaging Group [hep-ex/0412073].
- [7] P. Gambino and M. Misiak, Nucl. Phys. B **611**, 338 (2001); A. J. Buras, A. Czarnecki, M. Misiak, and J. Urban, Nucl. Phys. B **631**, 219 (2002).
- [8] J. Kaneko *et al.* (Belle Collaboration), Phys. Rev. Lett. **90**, 021801 (2003); B. Aubert *et al.* (BABAR Collaboration), Phys. Rev. Lett. **93**, 081802 (2004).

- [9] P. Colangelo *et al.*, Phys. Rev. D **53**, 3672 (1996).
- [10] A. Ali *et al.*, Phys. Rev. D **61**, 074024 (2000).
- [11] D. Melikhov, N. Nikitin, and S. Simula, Phys. Rev. D **57**, 6814 (1998).
- [12] T. M. Aliev *et al.*, Phys. Lett. B **400**, 194 (1997); T. M. Aliev, M. Savci, and A. Özpineci, Phys. Rev. D **56**, 4260 (1997); C. -H. Chen and C. Q. Geng, Phys. Rev. D **66**, 094018 (2002); H.-M. Choi, C. -R. Ji, and L.S. Kisslinger, Phys. Rev. D **65**, 074032 (2002); N. G. Deshpande and J. Trampetic, Phys. Rev. Lett. **60**, 2583 (1988); A. Faessler *et al.*, EPJdirect C **4**, 18 (2002); C. Greub, A. Ioannissian, and D. Wyler, Phys. Lett. B **346**, 149 (1995); C. Q. Geng and C. P. Kao, Phys. Rev. D **54**, 5636 (1996).
- [13] M. Zhong, Y.L. Wu, and W.Y. Wang, Int. J. Mod. Phys. A**18**, 1959 (2003).
- [14] B. Aubert *et al.* (BABAR Collaboration), Phys. Rev. Lett. **91**, 221802 (2003).
- [15] A. Ishikawa *et al.* (Belle Collaboration), Phys. Rev. Lett. **91**, 261601 (2003).
- [16] K. Abe *et al.* (Belle Collaboration), BELLE-CONF-0415 [hep-ex/0410006].
- [17] F. Krüger, L. M. Sehgal, N. Sinha, and R. Sinha, Phys. Rev. D **61**, 114028 (2000); Erratum-*ibid.* D **63**, 019901 (2001).
- [18] F. Krüger and E. Lunghi, Phys. Rev. D **63**, 014013 (2001).
- [19] G. Hiller and F. Krüger Phys. Rev. D **69**, 074020 (2004).
- [20] D. Acosta *et al.*, Phys. Rev. Lett. **93**, 032001 (2004); V.M. Abazov, *et al.*, Phys. Rev. Lett. **94**, 071802 (2005).
- [21] B. Aubert *et al.* (BABAR Collaboration), Nucl. Instrum. Methods A **479**, 1 (2001).
- [22] S. Agostinelli *et al.*, Nucl. Instrum. Methods A **506**, 250 (2003).
- [23] R.A. Fisher, Ann. Eugenics **7**, 179 (1936).
- [24] G.C. Fox and S. Wolfram, Phys. Rev. Lett. **41**, 1581 (1978).
- [25] Throughout this paper, wherever particle charge or flavor is specified, the charge conjugate particle is also implied.
- [26] T. Skwarnicki (Crystal Ball Collaboration), Ph.D. thesis, Cracow Institute of Nuclear Physics (1986), DESY F31-86-02.
- [27] The function is $f(x) \propto x\sqrt{1-x^2} \exp[-\zeta(1-x^2)]$, where ζ is a fit parameter and $x = m_{ES}/E_b^*$; ARGUS Collaboration, H. Albrecht *et al.*, Z. Phys. C **48**, 543 (1990).
- [28] Particle Data Group, S. Eidelman *et al.*, Phys. Lett. B**592**, 1 (2004).
- [29] B. Aubert *et al.* (BABAR Collaboration), Phys. Rev. Lett. **94**, 141801 (2005).